

# Theoretical modeling approach for adsorption of fibronectin on the nanotopographical implants

Xiangsheng Gao<sup>1</sup>, Yuhang Zhao<sup>1</sup>, Min Wang<sup>1</sup>, Chaozong Liu<sup>2</sup> and Jiajun Luo<sup>3</sup>

<sup>1</sup>Beijing Key Laboratory of Advanced Manufacturing Technology, Faculty of Materials and Manufacturing, Beijing University of Technology, Beijing, China

<sup>2</sup>Institute of Orthopaedic & Musculoskeletal Science, Division of Surgery & Interventional Science, University College London, London, UK

<sup>3</sup>Centre for the Cellular Microenvironment, University of Glasgow, Glasgow, UK

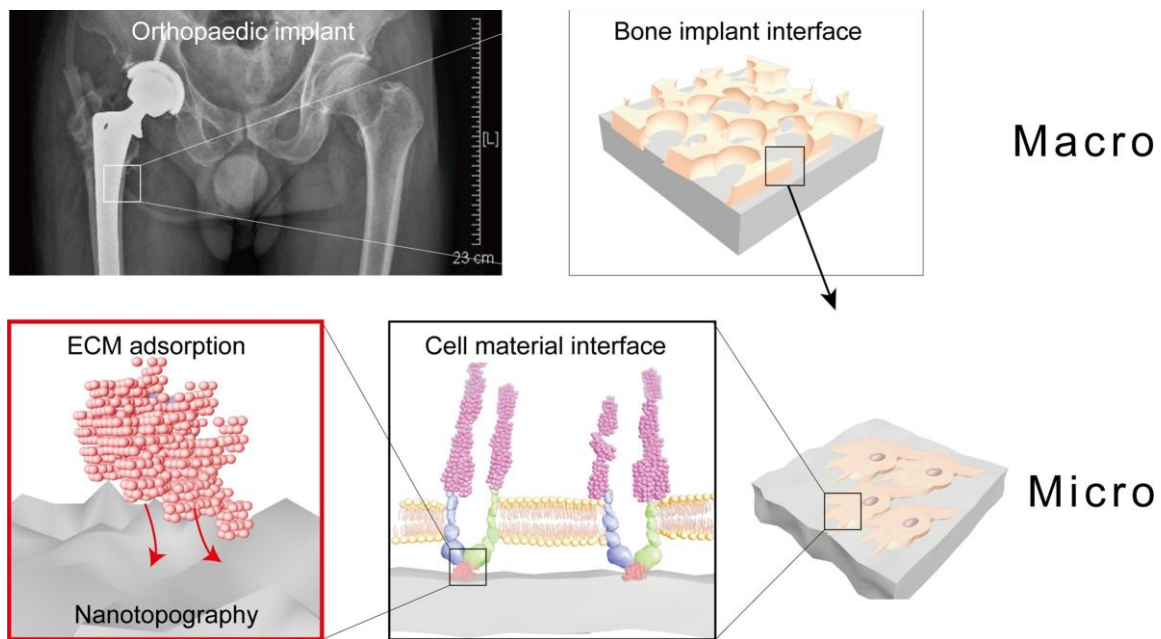
Corresponding authors:

Xiangsheng Gao, Beijing Key Laboratory of Advanced Manufacturing Technology, Faculty of Materials and Manufacturing, Beijing University of Technology, Pingleyuan 100, Beijing 100124, China.

Email: gaoxsh@bjut.edu.cn

Jiajun Luo, Centre for the Cellular Microenvironment, University of Glasgow, 79-85 Oakfield Avenue, Glasgow G12 8LT, UK.

Email: Jiajun.Luo@glasgow.ac.uk



In the macroscale, the combination between bone tissue and implant is dominated by the cellular responses to their microenvironment, which are initially influenced by the cell – extracellular matrix (ECM) interactions. The ECM adsorption on nanoscale Ti-topography is dominated by the Coulomb's force, we proposed a theoretical model to simulate multiple random fibronectin adsorption.

#### Abstract

The success of orthopedic implants depends on the sufficient integration between tissue and implant, which is influenced by the cellular responses to their microenvironment. The conformation of adsorbed extracellular matrix is crucial for cellular behavior instruction via manipulating the physiochemical features of materials. To investigate the electrostatic adsorption mechanism of fibronectin on nanotopographies, a theoretical model was established to determine surface charge density and Coulomb's force of nanotopography – fibronectin interactions using a Laplace equation satisfying the boundary conditions. Surface charge density distribution of nanotopographies with multiple random fibronectin was simulated based on random number and Monte Carlo hypothesis. The surface charge density on the nanotopographies was compared to the experimental measurements, to verify the effectiveness of the theoretical model. The model was implemented to calculate the Coulomb's force generated by nanotopographies to compare the fibronectin adsorption. This model has revealed the multiple random quantitative fibronectin electrostatic adsorption to the nanotopographies, which is beneficial for orthopedic implant surface design.

Significance: The conformation and distribution of adsorbed extracellular matrix on biomedical implants are crucial for directing cellular behaviors. However, the Ti nanotopography-ECM interaction mechanism remains largely unknown. This is mostly because of the interactions that are driven by electrostatic force, and any experimental probe could interfere with the electric field between the charged protein and Ti surface. A theoretical model is hereby proposed to simulate the adsorption between nanotopographies and fibronectin. Random number and Monte Carlo hypothesis were applied for multiple random fibronectin simulation, and the Coulomb's force between nanoconvex and nanoconcave structures was comparatively analyzed.

#### Keywords

Nanotopography, Coulomb's force, charge density, protein adsorption, bone implant interface

## Introduction

In the past few decades, the demand for orthopedic implants has been growing rapidly, especially in trauma, osteoporosis, bone cancer, joint and spine diseases, etc.<sup>1</sup> Success in application of orthopedic implants depends on surgeon, patient, and implant factors.<sup>2</sup> Two leading factors cause implant failure. The first is the lack of adequate adhering of bone tissue to implant surface, which leads to biomechanical loosening. The other failure is infection caused by biofilm formation at the bone implant interface. Both failures are caused by the lack of bonding at the bone-implant interface.<sup>3-5</sup> Indeed, the success of an implant biomaterial in microscale depends on factors of topological features, chemical composition, and mechanical properties, which co-influence cellular behaviors, such as adhesion, spreading, differentiation, and proliferation of cells.<sup>6</sup> Surface modification is an effective approach<sup>7</sup> to improve cell adhesion, bone tissue differentiation and regeneration, and biomechanical performance of implants.<sup>8-10</sup> Nanoscale roughness has been reported to have a great effect on protein adsorption,<sup>11</sup> thus generating nanotopography on the surface of implants is a feasible strategy to manipulate cell responses and avoid changing the chemical and mechanical features of Ti-based implants.<sup>12,13</sup>

Cell adhesion to biological materials is crucial at the initial stage of bone implant contact.<sup>14</sup> The interactions between tissue-implant in the macroscale and cells-implant in the microscale are illustrated in Figure 1. In the macroscale, the combination between bone tissue and implant is dominated by the cellular responses to their microenvironment, which are initially influenced

by the cell – extracellular matrix (ECM) interactions.<sup>15</sup> Specifically, cell adhesion to implant surface is achieved due to the interaction between the surface microfeatures and cellular receptors, such as integrin receptor to arginine-glycine-aspartic (RGD) sequences on fibronectin (FN) (ECM, red box in Figure 1).<sup>16</sup> FN can directly influence the behavior of integrin receptors and trigger downstream pathways.<sup>17,18</sup>

Protein adsorption is regulated by several factors, namely hydrophobicity/hydrophilicity, surface free energy, pH of adsorbing environment, charge of protein, and topographical features of the surface.<sup>19-22</sup> Therefore, manipulating the surface of implants in nanoscale has attracted the attention of researchers because it can create a topographical niche that regulates protein adsorption<sup>23,24</sup> and further influences cell behaviors, such as affecting the gene expression of osteoblasts.<sup>25</sup> The adsorption is caused by the electrostatic interaction between charged proteins and implant surface.<sup>26,27</sup> The electrostatic force can be manipulated by nanotopographical features to enhance osteoblast adhesion.<sup>28-30</sup> In particular, the electrostatic adsorption can be obtained by linearizing the finite difference Poisson-Boltzmann equation algorithm.<sup>31</sup> Kabaso et al.<sup>27</sup> and Asthagiri and Lenhoff<sup>32</sup> adopted an algorithm to further show that implants and osteoblasts are electrostatically attracted when the surface charge density reaches the threshold. Aiming to investigate the interactive attraction of implant surface charge density and electric field strength, Gongadze et al.<sup>33</sup> established a model based on highly curved edges of titanium surfaces and calculated the electric field strength using the Laplace equation. Their study showed that nano-scale

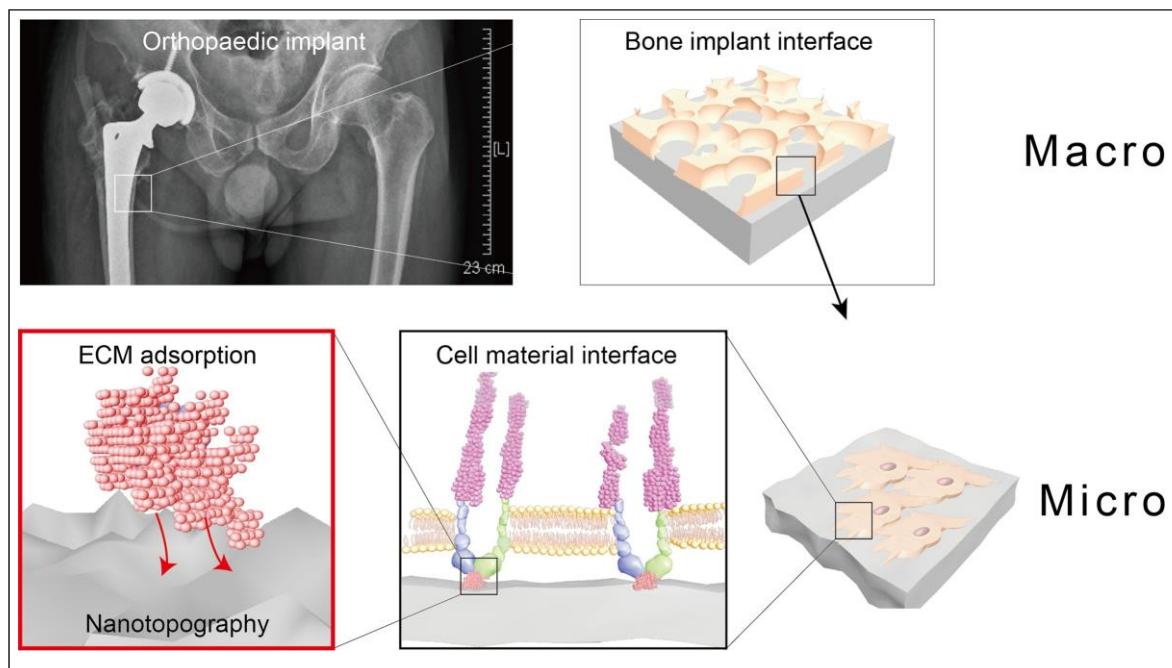


Figure 1. Implants at different scales. Bone implant integration in the macroscale is dominated by cell behaviors in the microscale.

regions on the titanium sharp edges and spikes may promote the adhesion of osteoblasts. The different adsorption mechanisms between nanoconvex and nanoconcave surfaces have been demonstrated in previous work, which further influence the human osteoblast adhesion.<sup>30</sup> Regards the adsorption mechanisms, Canpolat and Tatlısoz<sup>34</sup> presented a model for protein adsorption within a charged silica nanoparticle with an electrical double layer using finite element analysis. Atif et al.<sup>35</sup> used a Langmuir isotherm-based model to characterize protein and cell adhesion on a biomimetic hydroxyapatite surface. The equations were discretized in the time dimension and solved numerically using finite element method. Ercan et al.<sup>36</sup> proposed a linear regression-based protein adsorption model. Canpolat and Tatlısoz<sup>37</sup> also simulated the adsorption of a protein on a structured-nanoparticle by considering the charge regulation by using COMSOL Multiphysics. However, the efficiency of the finite element method is relatively low. Lubarsky et al.<sup>38</sup> showed that electrostatic force is an important driver (attraction or repulsion) for protein adsorption. The steric adsorption can be precisely controlled by designing electrostatic field distribution on the surface and by tuning the isoelectric points of the proteins.

Based on the electro-interaction between nanotopographies and proteins, a realistic model was established aiming to simulate the adsorption mechanisms of multiple FN and nanotopographies (nanoconvex and nanoconcave) via variation of Coulomb's force. Specifically, a nanotopographical model with charge density distribution and Coulomb's force was established. The charge density distribution in two conditions of FN adsorption was further simulated. The first hypothesis was based on random number of FN, and the other on

Monte Carlo simulation. The simulation results were comparatively analyzed with the experimental measurements from atomic force microscopy (AFM). The model to calculate Coulomb's force was implemented to compare the Coulomb's force between FN and different nanotopographies. Furthermore, the effect of nanotopographical diameter on the adsorption of nanoconvex structures was compared. Compared with our previous theoretical model,<sup>30</sup> the current model was developed by achieving proteins' randomness and multiple nanotopographies-protein interactions, thus improved the model's reliability.

## Material and methods

### *Modeling of Coulomb's force between nanotopographies and fibronectin*

The charge density is the key factor in protein adsorption and can be regulated by nanotopographies' features.<sup>33</sup> Inspired by this, nanotopographies were selected to adjust the charge distribution, affecting the protein adsorption. The electric field of charged nanotopographies is usually determined by the Poisson equation derived from the Maxwell equations of the electrostatic field. The Poisson equation is expressed as follows:

$$\nabla^2 \mathbf{u} = -\frac{\rho}{\epsilon} \quad \delta 1 \text{p}$$

Because the free charge is only distributed on the surface of the nanotopography, the charge inside the nanotopography is zero. Thus, the Poisson equation for this situation can be simplified as the Laplace equation, expressed as follows:

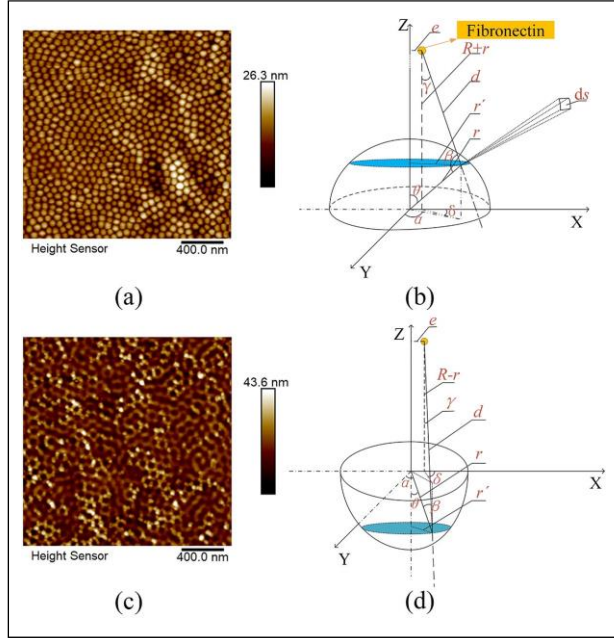


Figure 2. AFM morphological characteristics and geometric model characteristics of nanopographies: (a) the morphological characteristics of nanoconvex surface, (b) geometric schematic diagram of a single nanoconvex surface, (c) morphological characteristics of nanoconcave surface, and (d) geometric schematic diagram of a single nanoconcave surface.

$$\mathbf{r}^2 \mathbf{u} = 0 \quad \delta 2b$$

The electric field determination of the charged nanopography is transformed into a solution for the Laplace equation satisfying specific boundary conditions. Since the nanopographies are spherical crown in shape (Figure 2), the Laplace equation in spherical coordinates can be established and solved by the method in our previous research.<sup>30</sup>

In the initial state, the electric fields  $E_{r0}$  and  $E_{u0}$  with respect to radius  $r$  and polar angle  $u$  can be described as:

$$E_{r0} = -\frac{\partial u}{\partial r} = \frac{b_0}{r^2} + \frac{b_1}{r^3} \cos u \quad \delta 3b$$

$$E_{u0} = -\frac{\partial u}{\partial u} = \frac{b_1}{r^2} \sin u \quad \delta 4b$$

Combining of the two components of the field strength at a specific point, yields the initial electric field strength  $E_0$  at a specific point on the surface of the nanopography as:

$$E_0 = \sqrt{E_{r0}^2 + E_{u0}^2} \quad \delta 5b$$

According to the relationship between the electric field strength and the surface charge density, the charge

density at a specific point on the nanopography in the initial state can be obtained as:

$$S_0 = eE_0 \quad \delta 6b$$

where  $e$  is the dielectric constant.

Without the influence of charged proteins, the distribution of the electrons on the surface of the nanopographies is uniform. In this situation, the charge density on the surface of the structure is  $S_0$ . Considering charged FN around the nanopography, the free electrons on the surface of nanopographies redistribute and reach equilibrium again. It is noted that conformational changes of the protein were not considered. The conformational changes of proteins are at lower dimensions compared to the nanopography, which is in nanoscale. In nanoscale, the distribution of proteins is the principal consideration in this research.

Following the influence of FN, the redistributed electric field strength will be changed on the basis of the initial field strength, and the redistributed field strength can be described as:

$$E_{r1} = E_{r0} + E_r^{\delta} \quad \delta 7b$$

$$E_{u1} = E_{u0} + E_u^{\delta} \quad \delta 8b$$

where,  $E_r^{\delta}$  is the field strength increment along the radial direction of the nanopography surface affected by charged FN and  $E_u^{\delta}$  is the field strength increment along the polar direction of the nanopography surface. The detailed modeling process for nanoconcave and nanoconvex structures is illustrated in Supporting Information.

### Model effectiveness verification

The surface charge density distribution of a single nanopography affected by multiple randomly distributed FN was compared with the experimentally measured potential.

**Nanoconvex structure.** From the geometric relationship of a single nanopography affected by multiple random FN, depicted in Figure 3, the coordinate of a random FN can be expressed as  $(x, y, z)$ , and the coordinate of the diminutive surface on the nanoconvex structure can be expressed as  $(r \sin u \sin a, r \sin u \cos a, r \cos u)$ . The distance  $d$  between FN and the diminutive surface is expressed as shown in equation (9):

$$d = \sqrt{(x - r \sin u \sin a)^2 + (y - r \sin u \cos a)^2 + (z - r \cos u)^2} \quad \delta 9b$$

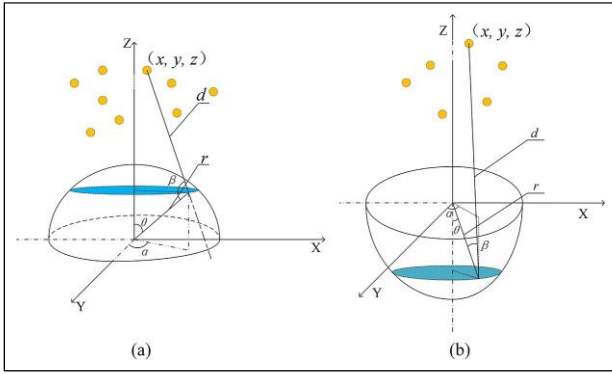


Figure 3. Geometric relationship between multiple random proteins and a single nanotopography: (a) nanoconvex and (b) nanoconcave.

Similarly, the distance between FN and the origin can be expressed as  $\sqrt{x^2 + y^2 + z^2}$ , so the angle  $b$  between the radius and the straight line which connects the FN and the diminutive surface can be obtained as follows:

$$b = \arccos \frac{\sqrt{r^2 + d^2 - x^2 - y^2 - z^2}}{2rd} \quad (10)$$

According to the proposed theoretical model, the electric field intensity distribution on the nanoconvex surface can be obtained, considering the influence of multiple random proteins, and the surface charge density redistribution can also be obtained. The redistributed and normalized nano-surface charge density  $S_1$  is obtained from equation (11).

$$S_1 = \frac{Q_{t0}}{Q_{t1}} S_0 \quad (11)$$

where  $Q_{t0}$  is the total surface charge before redistribution,  $Q_{t1}$  is the total surface charge after redistribution considering multiple random proteins, and  $S_0$  is the surface charge density in the initial state before

redistribution.

**Nanoconcave structure.** The coordinate of a single random FN in the nanoconcave structure was similar to that in the nanoconvex structure, expressed as  $(x, y, z)$ . The diminutive surface on the nanoconcave structure is expressed as  $(r \sin u \sin a, r \sin u \cos a, 2r \cos u)$  in this coordinate system and the distance between them is as follows:

$$d = \sqrt{(x - r \sin u \sin a)^2 + (y - r \sin u \cos a)^2 + (z - 2r \cos u)^2} \quad (12)$$

The determination process of the charge density on the nanoconcave structure affected by multiple random FN was the same as that on the nanoconvex structure.

## Results and discussion

### Model verification

**Numerical results based on random number simulation.** When FN was randomly distributed, the charge density distribution on surface also varied with the distribution of FN. Three cases with 30, 40, and 50 random FN were selected to be compared. Numerical simulations based on random numbers were performed multiple times to obtain the charge density distributions in different random states (Figures 4 and 5).

The number of random proteins affects the surface charge density. The charge density distribution in case 1 was significantly different, a large randomness was observed and the charge density could not be accurately predicted (Figure 4(a)). The charge density in case 2 was stabler, the charge concentration was basically on the top of the nanoconvex surface, with this concentration trend being more obvious in case 3. The charge density distribution in Figure 5(a) showed that the charge density distribution on the nanoconcave structure had a large uncertainty and the charge density distribution on nanoconcave structure was generally irregular. The top of the nanoconvex surface had a high-density charge at the location closest to the FN (Figure 4(a)). However, in the case of the nanoconcave surface, the charge at the edge with the minimum distance was relatively scattered (Figure 5(a)).

To compare the number of FN on the surface charge density in different random states, the three cases were randomly calculated 25 times. Then the charge density error of the nanoconvex surface after each randomization was calculated as:

$$Er = \frac{\sum_{i=1}^n (S_i^1 - S_i^2)^2}{S_i^1 + \dots + S_i^1} \quad (13)$$

where  $S_n^1$  and  $S_n^2$  are the charge densities of the diminutive surface at the same location for different cases. The errors were calculated according to equation (13) as shown in Figure 4(c).

The error analysis in Figure 4(c) shows that when the number of random FN was 30 and 40, the errors of the charge density distribution in different random states were relatively higher. Among the 25 random states, there were multiple errors of more than 4% and one more than 5%. The charge density distribution errors caused by 40 and 50 random proteins were smaller. In particular, they were less than 4% and the maximum error was 5% in the majority of states. When the number of random proteins was 30, the distribution of charge density on the nanotopography

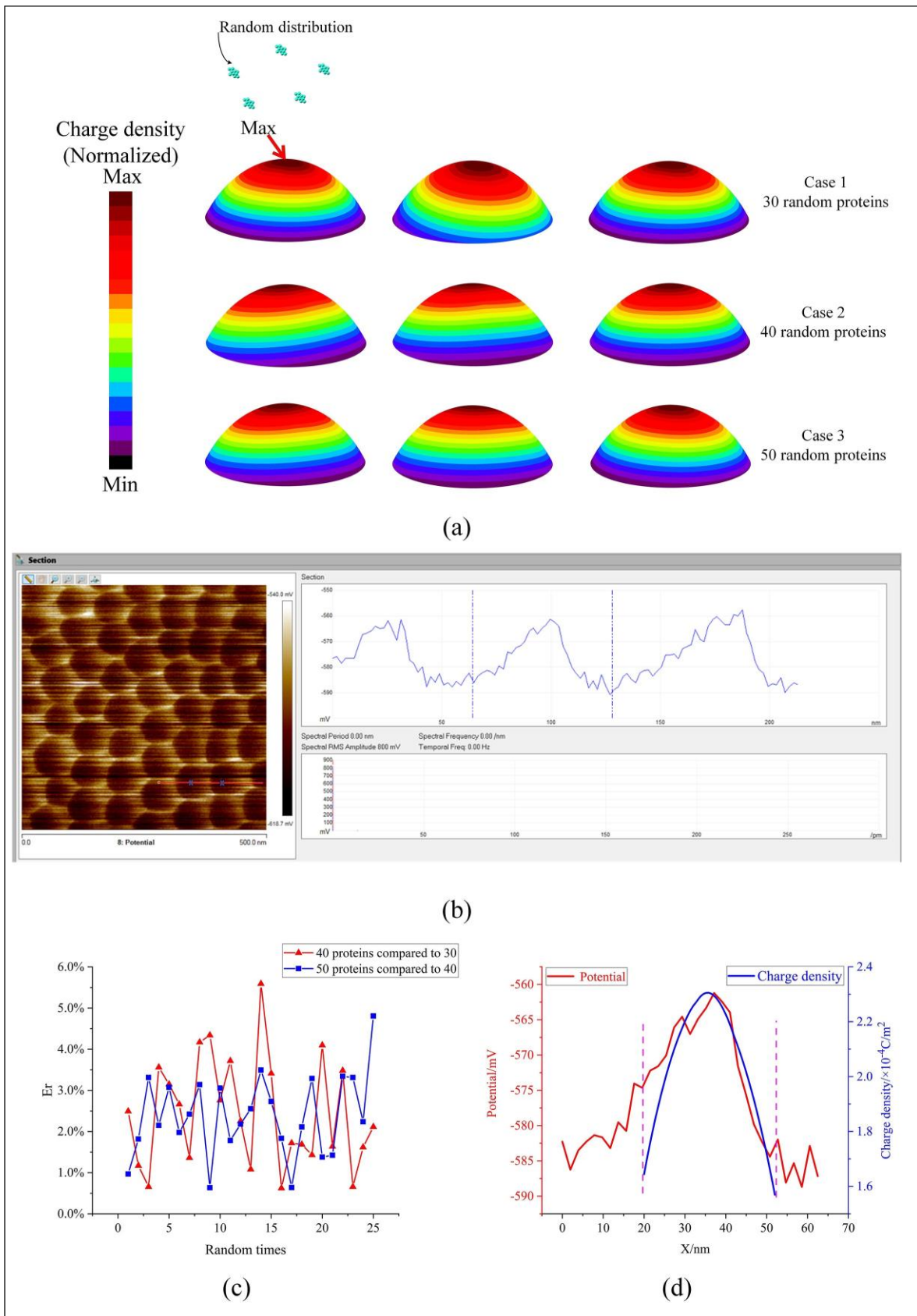


Figure 4. Numerical and experimental analysis of nanoconvex structures: (a) surface charge density distribution of the nanoconvex surface influenced by different amounts of random FN, (b) experimental results of the nanoconvex structure, (c) nanoconvex surface charge density distribution errors influenced by different amounts of FN in different random states, and (d) comparison of theoretical calculation and experimental results.

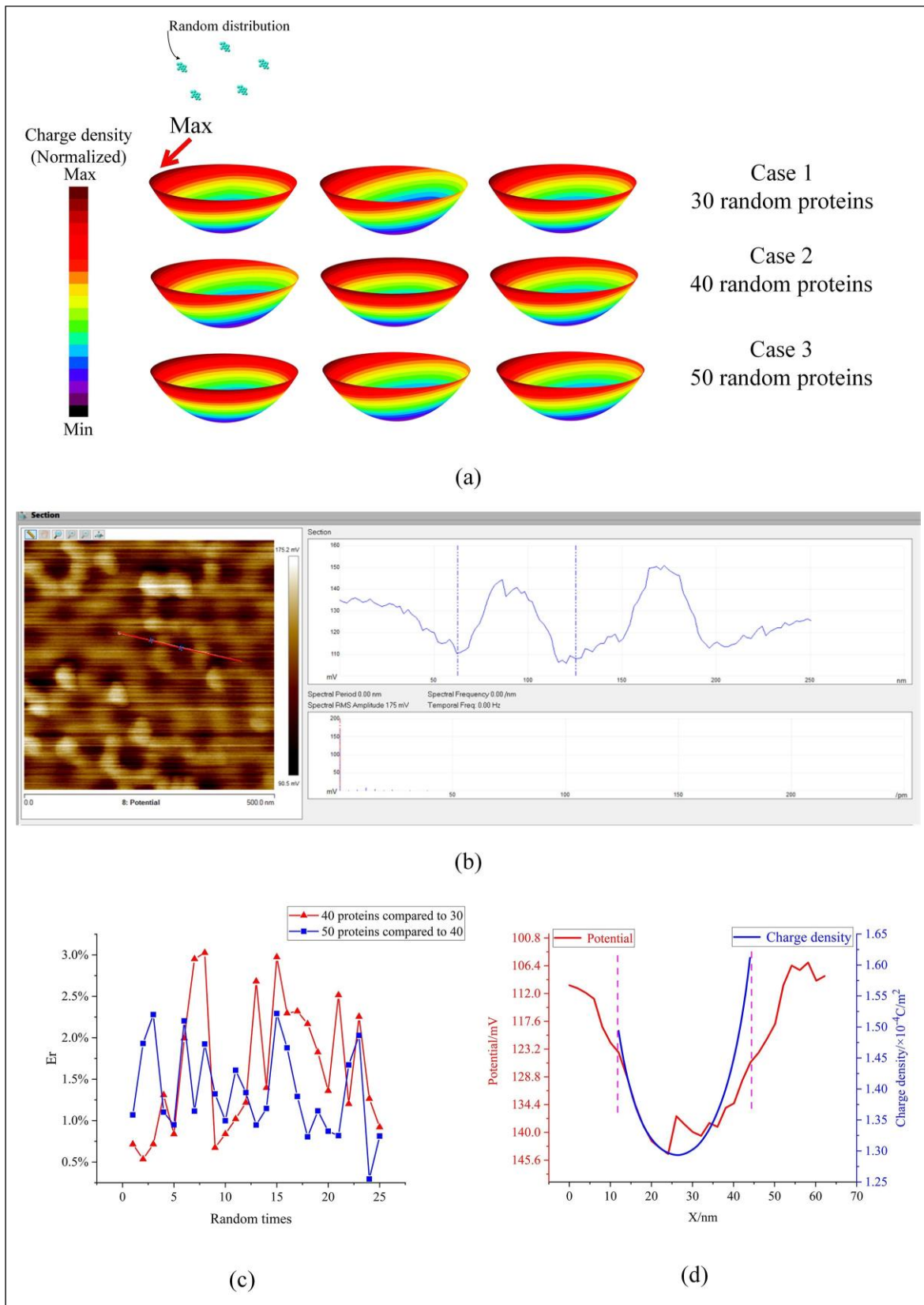


Figure 5. Numerical and experimental analysis of nanoconcave structures: (a) surface charge density distribution of the nanoconcave surface influenced by different amounts of random FN, (b) experimental results of the nanoconcave structure, (c) nanoconcave surface charge density distribution errors influenced by different amounts of FN in different random states, and (d) comparison of theoretical calculation and experimental results.



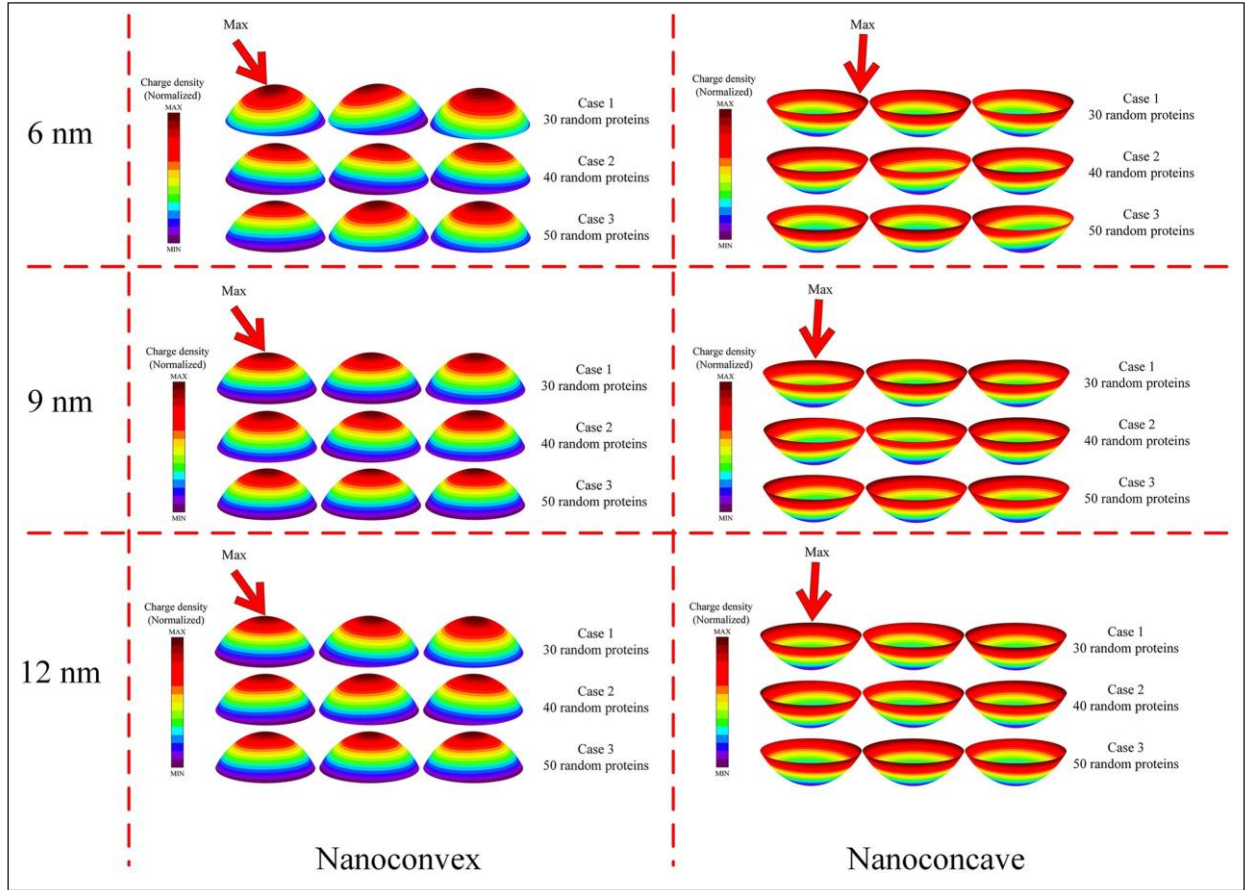


Figure 6. Charge density distribution of nanopopographies under limit distances with 6, 9, and 12 nm by Monte Carlo simulation.

surface was closely related to the position of FN, and the charge density distribution in this situation had a large randomness that could not be predicted. In the case of 40 proteins, the nanopopography surface charge density became less random and more concentrated on top of the nanoconvex surface due to the increased number of FN. As the protein number reached 50, the charge density distribution had no significantly randomly changed, compared with 40 random proteins.

Similarly, the charge density distribution errors for nanoconcave structures affected by different numbers of random FN are presented in Figure 5(c). The influence of FN number on the charge density distribution of the nanoconcave surface was smaller than that of the nanoconvex one.

The numerical results were compared with the experimental results, to verify the proposed theoretical model. The potential on the nanopopography was measured by AFM. To ensure accuracy of the experimental results, a point on the edge of the nanopopography surface was assigned potential zero. Then, the potential on the nanopopography on a line along the radial direction was measured, and the potential curve was obtained as shown in Figures 4(b) and 5(b). The effectiveness of this model can be verified by comparing the potential of a nanopopography on the curve (the truncated part in Figures 4(b) and 5(b)) with the theoretical charge density.

In Figures 4(d) and 5(d), the red curve is the potential intercepted from the experimental result, and the blue curve is the charge density distribution determined according to the proposed model. A single nanoconvex structure can be regarded as an isolated conductor, and the relationship between its charge and voltage can be obtained as:

$$U = \frac{Q}{C} = \frac{S}{C} \rho \quad (14)$$

where  $Q$  is the charge,  $C$  is the capacitance of the nanoconvex structure, and  $S$  is the area of the required charge.

Equation (14) shows that when the area and capacitance are constant, the voltage is proportional to the charge density. The surface of nanopopographies was negatively charged, featured with inversely proportional. Therefore, the formula shows that the higher the charge density, the lower the voltage and the lower the absolute value of the potential are.

Comparison between the simulation and the experiment of the nanoconvex structure in Figure 4(d) shows the voltage at the top of the nanoconvex structure was lower than the voltage at the bottom. Due to the negative charge being concentrated on the top, and the absolute value of the potential on the top was smaller than that at the bottom. Thus, the higher the charge

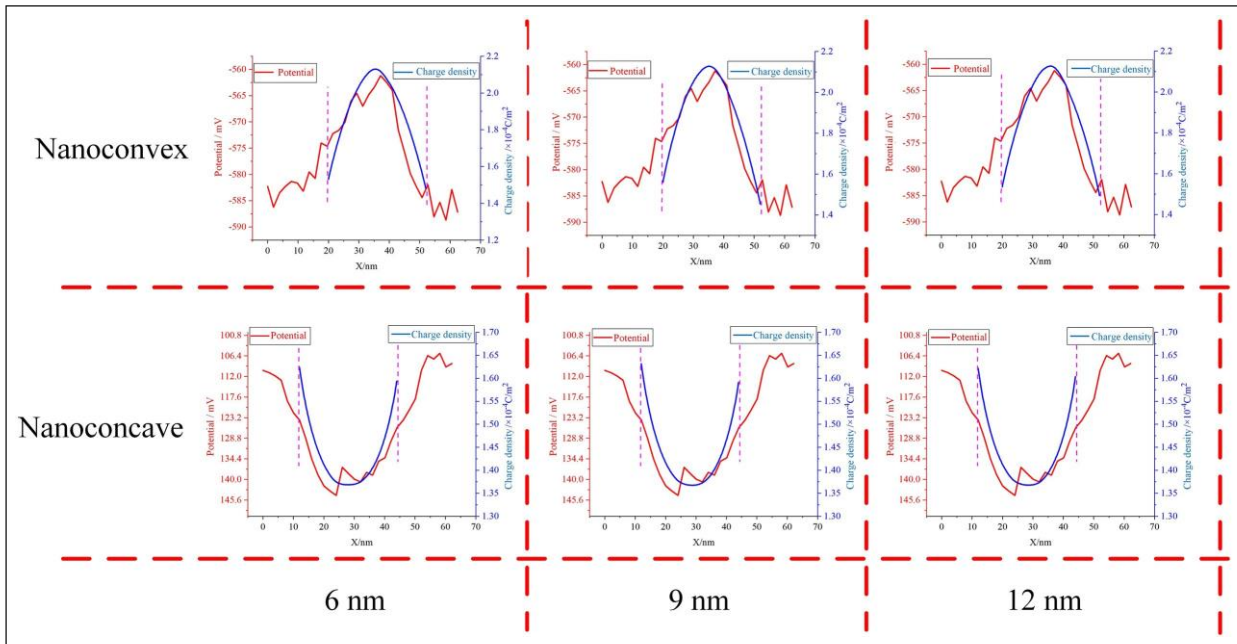


Figure 7. Comparison of experimental results and the results from Monte Carlo simulation.

density, the lower the voltage and the lower the absolute value of the potential are. Similarly, Figure 5(d) shows that the absolute value of the potential was lower at the region with higher charge density on the nanoconcave surface, and the distribution followed an inversely proportional relationship. The charge density curve obtained by theoretical simulation was basically consistent with the experimental results. Therefore, it could be concluded that the proposed model is able to predict the charge density distribution on the nanotopography surface.

*Numerical results based on Monte Carlo simulation.* Random simulations were able to simulate the protein distribution in a completely random state. However the distribution of FN above the nanotopography was not a completely random state. Other constraints that affect the random states of proteins need to be discussed. The Monte Carlo random simulations were carried out based on the constraints. In nanoscale, a cluster of protein molecules was considered as a point charge, so a minimum limiting distance in nanometers between the two point charges needed to be considered in the random process, to efficiently simulate the distribution of proteins. The limit distance was determined by the electrostatic repulsion between the two point charges. When the distance was less than the limit distance, a large electrostatic repulsion between the two point charge manifests, making the proteins are unstable. Due to the electrostatic repulsion, the proteins undergo relative motion until electrostatic repulsion is no longer presented between them, that is, the distance between the two point charges is greater than or equal to the limit distance. The exact value of this limit distance has not been explicitly reported in existing studies and was

ignored,<sup>27</sup> until the effect of the limit distance between two proteins that generate electrostatic repulsion is no longer considered. In order to represent the electrostatic repulsion of the proteins' random distribution, the Monte Carlo randomization was employed in the simulation of FN distributions. Random distribution of proteins at different limiting distances was considered. According to the mathematical model, the nano-surface charge density distribution under multiple proteins randomly distributed by Monte Carlo simulation was obtained. Three different limit distances of 6, 9, and 12 nm were compared and the comparison results are shown in Figures 6 and 7.

The results obtained by Monte Carlo random simulations were generally close to the results in Section "Numerical results based on random number simulation." For the nanoconvex structure, the high concentration of charge density was essentially distributed on the top, because the charges were subjected to protein attraction. Comparison with the experimental results showed that the charge density distribution on the nanotopography, the results of multiple random proteins by Monte Carlo simulation were basically consistent. Regarding the limit distance between multiple FN, the simulation results showed the negligible effect on the nano-surface charge density distribution.

### *Coulomb force analysis of different nanotopographies*

Based on the theoretical model, numerical simulations were performed to evaluate the effect of the nanotopography on Coulomb force and the nanotopography diameter effects on Coulomb force.

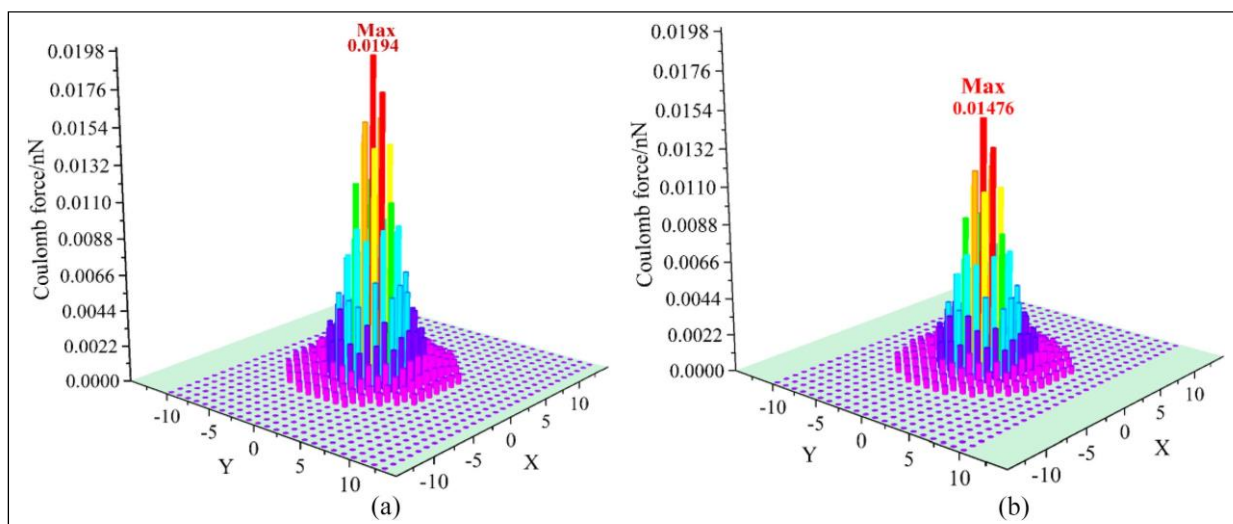


Figure 8. Coulomb force between the entire surface of nanotopographies and FN: (a) nanoconvex and (b) nanoconcave.

Table 1. Total Coulomb force of different nanotopography.

Nanotopography	Nanoconvex surface	Nanoconcave surface
Total Coulomb's force (nN)	0.32	0.23

Since each nanoconvex/nanoconcave surface has an adsorption effect on proteins, the adsorption effect on FN was ignored if Coulomb forces were less than 10% of the maximum Coulomb force. According to the model, the vertical Coulomb force that had the effects on the protein attraction was selected for comparison.

Coulomb force of a single FN and the entire nanotopography is shown in Figure 8. Each cylinder represents Coulomb force between a single nanoconvex/nanoconcave surface and an FN. It was concluded that for all qualified nanotopographies distributed in a circle around the FN, Coulomb force generated by nanoconvex structures was larger than that of nanoconcave ones. The dark purple regions in Figure 8 were ignored because Coulomb force was less than 10% of the maximum value. Coulomb force between each nanoconvex/nanoconcave and FN was accumulated to obtain a total Coulomb force between the entire nanotopographical surface and FN, as shown in Table 1. It was concluded that the total Coulomb force of nanoconvex surfaces was 39% larger than that of the nanoconcave ones.

### Coulomb's force analysis of nanoconvex surfaces with different diameters

Due to the different curvatures leading to the inhomogeneous charge distribution, the surface charge density is affected by nanotopographical dimensions,<sup>34</sup>

subsequently influencing the FN adsorption. The influence of nanoconvex diameter on FN adsorption was investigated. With the same offset of the FN, the Coulomb force changes due to the variation of the nanoconvex diameter. Four diameters of nanoconvex surfaces with 15, 20, 30, and 50 nm were selected to compare the Coulomb's force with the 40 nm.

Coulomb force comparison between FN and entire surface of nanoconvex structures with different diameters is shown in Figure 9. The results show that the smaller the diameter, the higher the number of nanoconvex structures that satisfy the Coulomb force assumption is, and the smaller the Coulomb force of a single nanoconvex structure is. Among these diameters, Coulomb force of the 50 nm nanoconvex structure was the largest when single nanoconvex structure was considered. In order to clarify this trend, the Coulomb forces between the nanoconvex structures with different diameters/numbers and FN were calculated, as shown in Figure 10.

The total Coulomb force of the entire nanoconvex surface with different diameters on FN (based on Figure 9) was calculated and compared, as shown in Table 2.

Figure 9 and Table 2 show that the Coulomb force of a single nanoconvex structure with a 15 nm diameter was the smallest. However, the total Coulomb force between the entire area of the nanotopography with 15 nm diameter and FN was the largest.

The model has indicated that the smaller the diameters of the nanoconvex structure surface, the stronger the adsorption effect of the protein is. This is mainly because under the same area, the higher number of smaller diameter nanoconvex structures is higher than that with a larger diameter (Figure 10). Previous studies<sup>39-42</sup> have mentioned that in the relatively narrow nano-size range, the behavior of osteoblasts had changed, and small-diameter nanotopographies had more convex edges with high curvature, which might

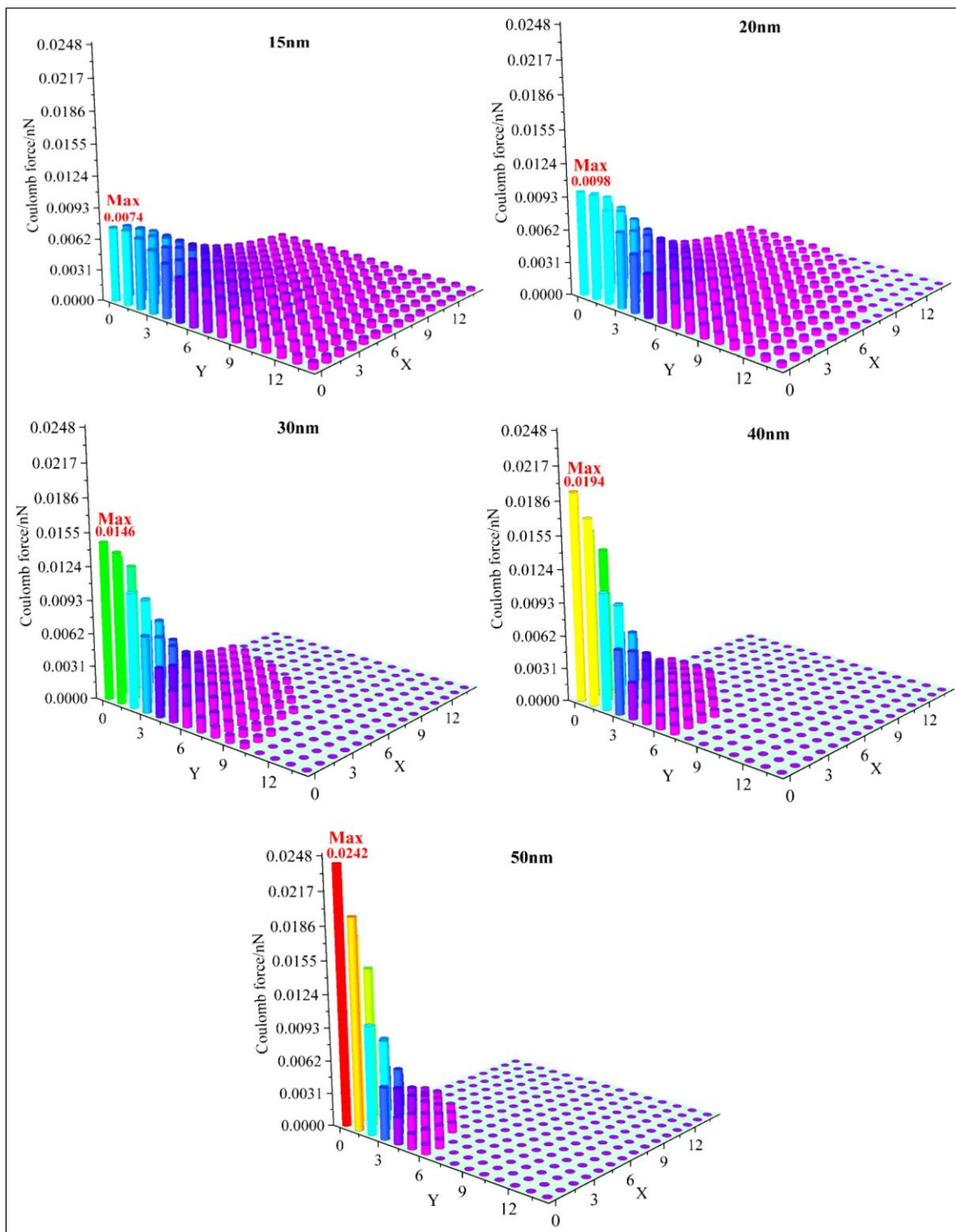


Figure 9. Coulomb's force between FN and nanoconvex structures with different diameters.

lead to higher amount of protein adsorption. Moreover, the convex edge with the small-diameter nanoconvex structure was sharper than that of the large-diameter, to increase the adhesion affinity of the

structure surface.<sup>43</sup> In summary, the surface of the nanoconvex structure with a diameter of 15 nm leads to a greater Coulombs force, and its protein adsorption effect is stronger.

Table 2. Total Coulomb's force of nanoconvex structures with different diameters.

Diameter	15 nm	20 nm	30 nm	40 nm	50 nm
Total Coulomb force (nN)	0.40	0.34	0.25	0.20	0.17

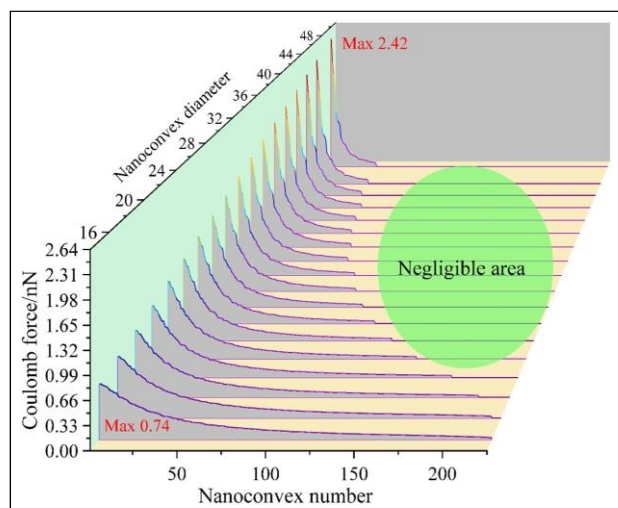


Figure 10. Coulomb's force between the various diameters of nanoconvex structures and FN.

## Conclusions

In this study, a theoretical method for determining Coulomb force was proposed to predict the random fibronectin (FN) adsorption on nanotopographies. The charge density distribution on the surface of the nanotopography and Coulomb force under different conditions were analyzed, producing the following conclusions.

- (1) When multiple FN were randomly distributed above the nanotopography, the charge density distribution of the nanotopography under the influence of the random proteins was obtained by random number and Monte Carlo simulations. The distribution was compared with the charge distribution obtained experimentally, and the effectiveness of this model was validated.
- (2) In terms of identical nanotopographies' diameter, the Coulombs force of single nanoconvex-FN was greater than single nanoconcave-FN. After Coulomb force was accumulated, it was estimated that the total Coulombs force between the entire nanoconvex surface and FN was 39% larger than that on the nanoconcave surface, which indicated that the nanoconvex structure had an enhanced adsorption capacity for FN.
- (3) With different nanoconvex diameters, it was found that the total Coulomb's force of small diameter nanoconvex surface – FN was more intense than large diameter nanoconvex surface – FN. In

specific, the surface of the nanoconvex structure with a diameter of 15 nm had a stronger adsorption force for FN.

Although a mathematical model of protein adsorption considering the randomness of proteins and the multiple nanostructures was established, however, the protein-protein interactions were not considered in this research. Therefore, future study can focus on the inclusion of protein-protein interactions. Additionally, surface wettability, topography, charge, and chemistry can deeply modify surface-protein interactions. Apart from this, protein conformations, such as structural stability, charge, and dimension, can also greatly affect adsorption. Other environmental factors that can influence adsorption include pH, ionic strength, protein concentration, protein mixture, and temperature of the solution.<sup>44</sup> Integration of these factors in the mathematical model will be the focus in the next stage of research work.

## Author contributions

X.G and J.L designed the study. Y.Z and X.G researched an appropriate model for simulation. M.W and C.L have supervised this work. X.G, Y.Z, and J.L wrote the article.


## Declaration of conflicting interests

The author(s) declared no potential conflicts of interest with respect to the research, authorship, and/or publication of this article.

## Funding

The author(s) disclosed receipt of the following financial support for the research, authorship, and/or publication of this article: This research is funded by National Natural Science Foundation of China, grant number 51875008; the EU via the H2020-MSCA-RISE-2016 program, grant number 734156; the international Research Cooperation Seed Fund of Beijing University of Technology (grant number: 2021A10).

## ORCID iD

Xiangsheng Gao  <https://orcid.org/0000-0001-5947-5826>

## Supplemental material

Supplemental material for this article is available online.

## References

1. Lin X, Yang S, Lai K, et al. Orthopedic implant biomaterials with both osteogenic and anti-infection capacities and associated in vivo evaluation methods. *Nanomedicine* 2017; 13(1): 123–142.
2. Wang W, Ouyang Y and Poh CK. Orthopaedic implant technology: biomaterials from past to future. *Ann Acad Med Singap* 2011; 40(5): 237–244.
3. Arciola CR, Campoccia D and Montanaro L. Implant infections: adhesion, biofilm formation and immune evaluation. *Nat Rev Microbiol* 2018; 16(7): 397–409.
4. Tomizawa T, Ishikawa M, Bello-Irizarry SN, et al. Biofilm producing *Staphylococcus epidermidis* (RP62A strain) inhibits osseous integration without osteolysis and histopathology in a murine septic implant model. *J Orthop Res* 2020; 38(4): 852–860.
5. Fernandez-Yague MA, Abbah SA, McNamara L, et al. Biomimetic approaches in bone tissue engineering: integrating biological and physicochemical strategies. *Adv Drug Deliv Rev* 2015; 84: 1–29.
6. Wang Y, Wen C, Hodgson P, et al. Biocompatibility of TiO<sub>2</sub> nanotubes with different topographies. *J Biomed Mater Res* 2014; 102(3): 743–751.
7. Florea DA, Albulea D, Grumezescu AM, et al. Surface modification – a step forward to overcome the current challenges in orthopedic industry and to obtain an improved osseointegration and antimicrobial properties. *Mater Chem Phys* 2020; 243: 122579.
8. Devgan S and Sidhu SS. Evolution of surface modification trends in bone related biomaterials: a review. *Mater Chem Phys* 2019; 233: 68–78.
9. Luo J, Tamaddon M, Yan C, et al. Improving the fretting biocorrosion of Ti<sub>6</sub>Al<sub>4</sub>V alloy bone screw by decorating structure optimised TiO<sub>2</sub> nanotubes layer. *J Mater Sci Technol* 2020; 49: 47–55.
10. Luo J, Li B, Ajami S, et al. Growth of TiO<sub>2</sub> nanotube on titanium substrate to enhance its biotribological performance and biocorrosion resistance. *J Bionic Eng* 2019; 16: 1039–1051.
11. Rockwell GP, Lohstreter LB and Dahn JR. Fibrinogen and albumin adsorption on titanium nanoroughness gradients. *Colloids Surf B Biointerfaces* 2012; 91: 90–96.
12. Hoyos-Nogue's M, Velasco F, Ginebra MP, et al. Regenerating bone via multifunctional coatings: the blending of cell integration and bacterial inhibition properties on the surface of biomaterials. *ACS Appl Mater Interfaces* 2017; 9(26): 21618–21630.
13. Luo J, Walker M, Xiao Y, et al. The influence of nanotopography on cell behaviour through interactions with the extracellular matrix - a review. *Bioact Mater* 2022; 15: 145–159.
14. Anselme K. Osteoblast adhesion on biomaterials. *Biomaterials* 2000; 21(7): 667–681.
15. Jung S, Bohner L, Hanisch M, et al. Influence of implant material and surface on mode and strength of cell/matrix attachment of human adipose derived stromal cell. *Int J Mol Sci* 2020; 21(11): 4110.
16. Raines AL, Berger MB, Schwartz Z, et al. Osteoblasts grown on microroughened titanium surfaces regulate angiogenic growth factor production through specific integrin receptors. *Acta Biomater* 2019; 97: 578–586.
17. Garcia AJ, Vega MD and Boettiger D. Modulation of cell proliferation and differentiation through substrate-dependent changes in fibronectin conformation. *Mol Biol Cell* 1999; 10(3): 785–798.
18. Keselowsky BG and Garcia AJ. Surface chemistry modulates integrin binding to direct cell adhesion and function. In: *Transactions of the 7th world biomaterials congress*, 2004, p.369.
19. Hasan A and Pandey LM. Surface modification of Ti<sub>6</sub>Al<sub>4</sub>V by forming hybrid self-assembled monolayers and its effect on collagen-I adsorption, osteoblast adhesion and integrin expression. *Appl Surf Sci* 2020; 505: 144611.
20. Chang HY, Kao WL, You YW, et al. Effect of surface potential on epithelial cell adhesion, proliferation and morphology. *Colloids Surf B Biointerfaces* 2016; 141: 179–186.
21. Attwood SJ, Kershaw R, Uddin S, et al. Understanding how charge and hydrophobicity influence globular protein adsorption to alkanethiol and material surfaces. *J Mater Chem B* 2019; 7(14): 2349–2361.
22. Metwally S and Stachewicz U. Surface potential and charges impact on cell responses on biomaterials interfaces for medical applications. *Mater Sci Eng C* 2019; 104: 109883.
23. Wu S, Liu X, Yeung KWK, et al. Surface nano-architectures and their effects on the mechanical properties and corrosion behavior of Ti-based orthopedic implants. *Surf Coat Technol* 2013; 233: 13–26.
24. Stevens MM and George JH. Exploring and engineering the cell surface interface. *Science* 2005; 310(5751): 1135–1138.
25. Perrotti V, Palmieri A, Pellati A, et al. Effect of titanium surface topographies on human bone marrow stem cells differentiation in vitro. *Odontology* 2013; 101(2): 133–139.
26. Hartvig RA, van de Weert M, Østergaard J, et al. Protein adsorption at charged surfaces: the role of electrostatic interactions and interfacial charge regulation. *Langmuir* 2011; 27(6): 2634–2643.
27. Kabaso D, Gongadze E, Perutkova S, et al. Mechanics and electrostatics of the interactions between osteoblasts and titanium surface. *Comput Methods Biomech Biomed Eng* 2011; 14(5): 469–482.
28. Wang Z, Yan Y and Qiao L. Protein adsorption on implant metals with various deformed surfaces. *Colloids Surf B Biointerfaces* 2017; 156: 62–70.
29. Gessner A, Lieske A, Paulke B, et al. Influence of surface charge density on protein adsorption on polymeric nanoparticles: analysis by two-dimensional electrophoresis. *Eur J Pharm Biopharm* 2002; 54(2): 165–170.
30. Luo J, Zhao S, Gao X, et al. TiO<sub>2</sub> nanotopography-driven osteoblast adhesion through Coulomb's force evolution. *ACS Appl Mater Interfaces* 2022; 14(30): 34400–34414.
31. Hlady V and Buijs J. Protein adsorption on solid surfaces. *Curr Opin Biotechnol* 1996; 7(1): 72–77.
32. Asthagiri D and Lenhoff AM. Influence of structural details in modeling electrostatically driven protein adsorption. *Langmuir* 1997; 13(25): 6761–6768.
33. Gongadze E, Kabaso D, Bauer S, et al. Adhesion of osteoblasts to a nanorough titanium implant surface. *Int J*

*Nanomedicine* 2011; 6: 1801–1816.

34. Canpolat C and Tatlısoz MM. Size-dependent protein adsorption on a nanoparticle. *IEEE Trans Nanobioscience* 2023; 22: 597–602.
35. Atif AR, La Cis U, Engqvist H, et al. Experimental characterization and mathematical modeling of the

- adsorption of proteins and cells on biomimetic hydroxyapatite. *ACS Omega* 2022; 7(1): 908–920.
36. Ercan B, Khang D, Carpenter J, et al. Using mathematical models to understand the effect of nanoscale roughness on protein adsorption for improving medical devices. *Int J Nanomedicine* 2013; 8 Suppl 1: 75–81.
  37. Canpolat C and Tatlisoz MM. Protein adsorption on a nanoparticle with a nanostructured surface. *Electrophoresis* 2022; 43: 2324–2333.
  38. Lubarsky GV, Browne MM, Mitchell SA, et al. The influence of electrostatic forces on protein adsorption. *Colloids Surf B Biointerfaces* 2005; 44(1): 56–63.
  39. Park J, Bauer S, von der Mark K, et al. Nanosize and vitality: TiO<sub>2</sub> nanotube diameter directs cell fate. *Nano Lett* 2007; 7(6): 1686–1691.
  40. Park J, Bauer S, Schmuki P, et al. Narrow window in nanoscale dependent activation of endothelial cell growth and differentiation on TiO<sub>2</sub> nanotube surfaces. *Nano Lett* 2009; 9(9): 3157–3164.
  41. Brammer KS, Oh S, Cobb CJ, et al. Improved bone-forming functionality on diameter-controlled TiO<sub>2</sub> nanotube surface. *Acta Biomater* 2009; 5(8): 3215–3223.
  42. Park J, Bauer S, Schlegel KA, et al. TiO<sub>2</sub> nanotube surfaces: 15 nm—an optimal length scale of surface topography for cell adhesion and differentiation. *Small* 2009; 5(6): 666–671.
  43. Gongadze E, Kabaso D, Bauer S, et al. Adhesion of osteoblasts to a vertically aligned TiO<sub>2</sub> nanotube surface. *Mini-Rev Med Chem* 2013; 13(2): 194–200.
  44. Barberi J and Spriano S. Titanium and protein adsorption: an overview of mechanisms and effects of surface features. *Materials* 2021; 14: 1590.